Chapter 2
Traction Power Generation with Tethered Wings

Roland Schmehl, Michael Noom, Rolf van der Vlugt

Abstract A tethered wing can be used in two different ways, to lift payload or to provide traction power. The latter is the basis of several innovative technical applications, such as kite-assisted ship propulsion and pumping-kite wind energy conversion. This chapter presents a theoretical analysis of traction power generation by a tethered wing, with the objective to establish the fundamental relationships between system and operational parameters on the one hand, and achievable mechanical power output on the other hand. In a first step, it is assumed that the instantaneous flight state of the wing can be approximated by the steady equilibrium of aerodynamic and tether forces. The analysis considers controlled flight along an arbitrary predefined trajectory, distinguishing the cases of varying tether length with fixed point anchoring and constant tether length with anchoring at a point moving in the ground plane. Theoretical results are compared with literature. In a second step, the analysis includes the effect of weight and centrifugal acceleration of the wing.

2.1 Introduction

The emerging use of kites for applications such as ship propulsion and electricity generation marks an interesting renaissance of a wind power technology that had been used for a variety of technical and scientific purposes until replaced by powered aircraft during the first half of the twentieth century [8]. In contrast to the historic use, which was mainly the lifting of payload, the current technical focus is on traction power generation. An example is shown in Fig. 2.1, which illustrates how advances in high-performance plastic materials, mechatronic systems including flight control and sensor technology, have contributed to the recent development. To achieve a high traction power, the wing is operated transverse to the tether in fig-

Roland Schmehl (✉) · Michael Noom · Rolf van der Vlugt
Delft University of Technology, Faculty of Aerospace Engineering, Kluyverweg 1, 2629HS Delft, The Netherlands, e-mail: r.schmehl@tudelft.nl

U. Ahrens et al. (eds.), *Airborne Wind Energy,* Green Energy and Technology,
DOI: 10.1007/978-3-642-39965-7_2, © Springer-Verlag Berlin Heidelberg 2013

Fig. 2.1 A remote-controlled 25m^2 Leading Edge Inflatable (LEI) tube kite flying crosswind while pulling a 4mm cable with a force of 3kN from the ground station swivel, generating a traction power of 15kW [8]

ure of eight or circular flight maneuvers. Compared to the stationary flight used for lifting payload, this maneuvered flight has the effect to substantially increase the relative wind velocity at the wing. Since the aerodynamic forces increase with the square of this velocity, the generated traction power rises accordingly. For example, at an average wind speed of 7m/s the transverse flight speed of the kite depicted in Fig. 2.1 varies between 20m/s and 25m/s, which clearly shows the dominating crosswind contribution to the traction force.

Compared to the constrained rotational motion of wind turbine blades, the kinematics of a maneuvering wing operated on a variable length tether is more complex. Furthermore, a reliable flight operation requires active control, not only to realize a specific flight path, but also to adjust the operation to variations in the wind environment and to avoid over- or underload of the airborne tensile structure. This can be particularly challenging for lightweight membrane wings which have a limited maximum wing loading and react rapidly to wind speed fluctuations. The increased technical complexity is, however, counterbalanced by the fact that the operation of a tethered wing can be adapted to a much larger extend to the available wind resource. For example, variations in the wind field can be compensated for by adjusting the operational altitude range and by making use of the fact that wind gets generally stronger and more persistent with increasing altitude.

Using the traction power of a tethered wing for large-scale electricity generation was first explored by Loyd [7]. The simplified steady flight analysis is restricted to the downwind direction and distinguishes two fundamental modes: the *simple kite*

which is moving only as a result of the extending tether, and the *crosswind kite* which is flying transverse to the wind velocity. Neglecting mass and assuming a straight tether, Loyd derives analytic expressions for the traction power when operating the simple kite at a constant elevation angle and the crosswind kite in the horizontal ground plane. An often quoted result of this study is the optimal reel-out speed calculated as $1/3$ of the wind speed. Wellicome [10] investigated the use of kites for ship propulsion. Assuming a straight tether of constant length, the steady flight analysis considers maneuvering of the kite on a spherical surface. Wellicome presents results for the amplification of the driving force by flying the kite in figure of eight maneuvers. These theories were generalized in subsequent studies, suspending several of the original simplifying assumptions [2, 6].

The objective of this chapter is to combine the existing approaches in a compact analytic theory which clearly indicates the influence of problem parameters and can be used for system-level design and optimization. Following the definition of the physical problem and the discussion of basic assumptions in Sect. 2.2, a universal formulation of the apparent wind velocity is derived in Sect. 2.3. In Sect. 2.4 the tangential kite velocity is defined as a generalization of the cross wind velocity. Assuming a massless kite, Sects. 2.5, 2.6 and 2.7 elaborate on traction power generation and Sect. 2.8 on ground vehicle propulsion. Sect. 2.9 extends the steady analytical framework by gravitational and inertial effects.

2.2 Problem definition and assumptions

The scope of this chapter is limited to the conversion of wind energy into traction power using a tethered wing. This mechanical power can be further converted, for example, into shaft power, by pulling the tether from a stationary drum. It can also be used directly to pull a moving ground vehicle. The basic physical problem is illustrated in Fig. 2.2, depicting the idealized state of a straight tether. Distributed external forces such as gravity and aerodynamic line drag will always lead to sagging of a flexible tether. However, in the traction phase the tether is generally fully tensioned and the tether force dominates the force equilibrium by orders of magnitude. Accordingly, the effect of sagging can be neglected, which is also visible from Fig. 2.1.

In practice, the type of wing can range from highly flexible membrane wing to rigid wing. For the purpose of this analysis the integral aerodynamic force $\mathbf{F}_a$ generated by the flying wing is approximated as the sum of a lift vector $\mathbf{L}$ and a drag vector $\mathbf{D}$

$$\mathbf{F}_a = \mathbf{L} + \mathbf{D}, \tag{2.1}$$

with the magnitudes of these force vectors represented as

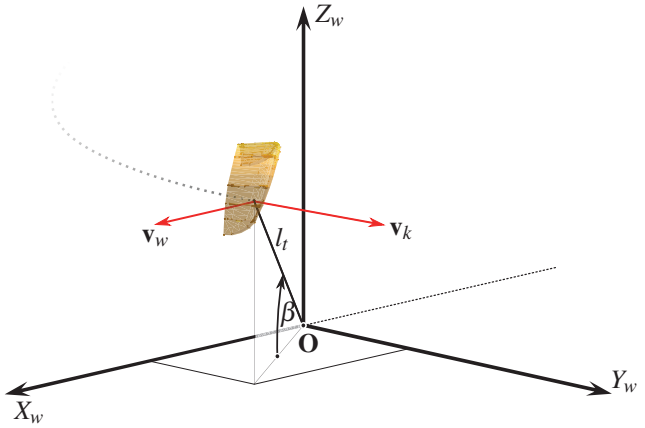

Fig. 2.2 A kite flying with velocity $\mathbf{v}_k$ on a straight tether of variable length l_t at an elevation angle β. The origin $\mathbf{O}$ of the wind reference frame X_w, Y_w, Z_w is located at the tether attachment point and the axis X_w is pointing in the direction of the wind velocity $\mathbf{v}_w$.

$$L = \frac{1}{2}\rho C_L v_a^2 S, \tag{2.2}$$

$$D = \frac{1}{2}\rho C_D v_a^2 S, \tag{2.3}$$

where C_L and C_D are the aerodynamic lift and drag coefficients, respectively, ρ is the air density and S the surface area of the wing projected in the direction of the lift vector. The apparent wind velocity is defined as the relative velocity at the wing

$$\mathbf{v}_a = \mathbf{v}_w - \mathbf{v}_k. \tag{2.4}$$

For the purpose of deriving an analytic theory, the wind velocity $\mathbf{v}_w$ is assumed to be uniform and constant, parallel to the ground plane. The aerodynamic coefficients are assumed to be constant properties of the wing. In reality, however, C_L and C_D vary with the instantaneous angle of attack of the wing, which is measured between the mean chord of the wing and $\mathbf{v}_a$. For the purpose of developing a closed analytic model this effect is not accounted for.

Although tether sag is not considered in the analysis, the integral contribution of aerodynamic line drag can affect the flight motion of the wing significantly, especially for multi-line tether configurations. This aerodynamic force contribution can be approximated by adding a fraction of the integral line drag to the aerodynamic drag of the wing [2]. This simple and effective method is not explicitly described in this chapter.

It is further assumed that the various forces on the wing all act in a single point $\mathbf{K}$ and that the flight maneuvers of the wing can be approximated as a sequence of

steady state changes. It is a characteristic feature of the lightweight maneuvering traction wing, that the force equilibrium is generally dominated by the aerodynamic force $\mathbf{F}_a$ and the tether force $\mathbf{F}_t$. Steering of the wing is not taken into account for the steady analysis, assuming that the wing tracks a predefined flight path.

The effect of the gravitational force $\mathbf{F}_g$ increases for lower elevation angles, contributions of inertial forces $\mathbf{F}_i$ are relatively small along the tether, the major force axis. Gravitational and inertial force contributions are not considered within the analytic theory presented in this chapter. In Sect. 2.9 both contributions are taken into account in the frame of the steady description.

2.3 Apparent wind velocity

The motion of a wing that is operated on a variable length tether can be described in terms of two fundamental components. A component along the tether, which is controlled by the deployment of the tether from the ground station, and a component perpendicular to the tether, which is under the authority of the flight control system of the wing. A natural choice for the kinematic analysis of such a system are spherical coordinates with the origin **O** located at the tether exit point at the ground station and the radial coordinate r describing the geometrical distance to the kite **K**. This

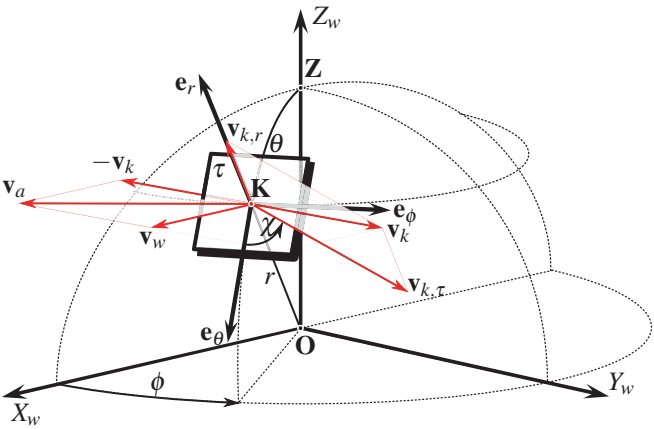

Fig. 2.3 Definition of the apparent wind velocity $\mathbf{v}_a = \mathbf{v}_w - \mathbf{v}_k$. Decomposition of the kite velocity $\mathbf{v}_k$ into radial and tangetial components $\mathbf{v}_{k,r}$ and $\mathbf{v}_{k,\tau}$, respectively. The course angle χ is measured in the tangential plane τ, the spherical coordinates (r, θ, ϕ) are defined with respect to the wind reference frame X_w, Y_w, Z_w.

configuration is illustrated in Fig. 2.3, showing the definition of polar angle θ and

azimuth angle ϕ. Alternatively to the polar angle the elevation angle $\beta = 90^\circ - \theta$ can be used. In spherical coordinates, the kite velocity can be decomposed into a radial component $\mathbf{v}_{k,r}$ and a tangential component $\mathbf{v}_{k,\tau}$

$$\mathbf{v}_k = \mathbf{v}_{k,r} + \mathbf{v}_{k,\tau}. \tag{2.5}$$

The direction of $\mathbf{v}_{k,\tau}$ in the tangential plane τ is quantified by the course angle χ, which is measured from the local base vector $\mathbf{e}_\theta$. Special cases are downwards flight ($\chi = 0$), upwards flight ($\chi = 180^\circ$) and horizontal flight ($\chi = 90^\circ$ and $\chi = 270^\circ$). Combining Eqns. (2.4) and (2.5) results in

$$\mathbf{v}_a = \mathbf{v}_w - \mathbf{v}_{k,r} - \mathbf{v}_{k,\tau}. \tag{2.6}$$

Using spherical coordinates (r, θ, ϕ) and the course angle χ as defined in Fig. 2.3 the apparent wind velocity $\mathbf{v}_a$ can be expressed as follows

$$\mathbf{v}_a = \begin{bmatrix} \sin\theta\cos\phi \\ \cos\theta\cos\phi \\ -\sin\phi \end{bmatrix} v_w - \begin{bmatrix} 1 \\ 0 \\ 0 \end{bmatrix} v_{k,r} - \begin{bmatrix} 0 \\ \cos\chi \\ \sin\chi \end{bmatrix} v_{k,\tau}. \tag{2.7}$$

Assuming a straight tether as discussed in Sect. 2.2 implies that the radial component of the kite velocity and the tether velocity are identical

$$\mathbf{v}_{k,r} = \mathbf{v}_t. \tag{2.8}$$

In order to normalize the tether velocity $v_t = \dot{r}$, the reeling factor is introduced as

$$f = \frac{v_t}{v_w}, \tag{2.9}$$

which is positive when the tether length increases. Accordingly, the tangential velocity factor is introduced to normalize the tangential component of the kite velocity

$$\lambda = \frac{v_{k,\tau}}{v_w}. \tag{2.10}$$

This non-dimensional parameter is a generalization of the cross wind factor which was introduced in [7] for the special case of horizontal flight ($\chi = 90^\circ$) in a downwind position ($\phi = 0$). For this case $\mathbf{v}_{k,\tau}$ is always perpendicular to $\mathbf{v}_w$. Using Eqns. (2.8)–(2.10), Eq. (2.7) can be expressed as

$$\mathbf{v}_a = \begin{bmatrix} \sin\theta\cos\phi - f \\ \cos\theta\cos\phi - \lambda\cos\chi \\ -\sin\phi - \lambda\sin\chi \end{bmatrix} v_w. \tag{2.11}$$

The apparent wind velocity can also be decomposed into radial and tangential components

$$\mathbf{v}_a = \mathbf{v}_{a,r} + \mathbf{v}_{a,\tau}. \tag{2.12}$$

The fundamental relation between the radial and tangential components of the apparent wind velocity and the lift and drag components of the aerodynamic force,

$$\frac{v_{a,\tau}}{v_{a,r}} = \frac{L}{D}, \tag{2.13}$$

can be derived from the geometrical similarity of the force and velocity diagrams illustrated in Fig. 2.4. This similarity can be explained as follows: vectors $\mathbf{v}_a$ and

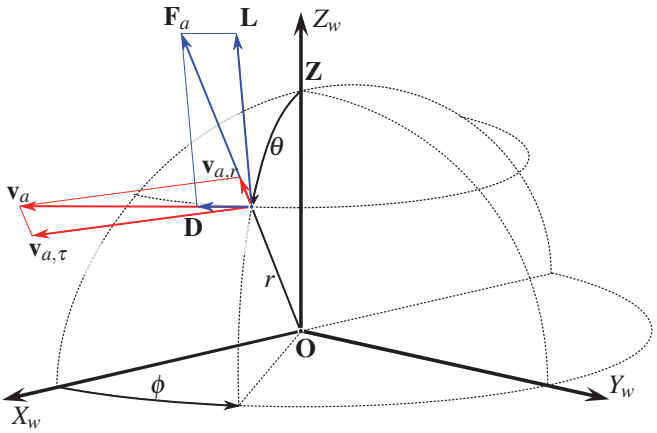

Fig. 2.4 Geometrical similarity of the force and velocity diagrams. $\mathbf{v}_a$ and $\mathbf{F}_a$ are decomposed in the plane spanned by the two vectors.

$\mathbf{F}_a$ span the plane in which both vectors are decomposed. The aerodynamic drag component **D** is aligned with $\mathbf{v}_a$ by definition. The radial component $\mathbf{v}_{a,r}$ is aligned with $\mathbf{F}_a$ as consequence of the straight tether assumption. The two alignments are the reason for the geometric similarity.

Equation (2.13) corresponds to [2, Eq. (19)] and to [7, Eq. (11)] for the special case of $\phi = 0$. The radial component of the apparent wind velocity follows from Eq. (2.11) as

$$v_{a,r} = (\sin\theta\cos\phi - f)v_w. \tag{2.14}$$

Combining Eqns. (2.12)–(2.14) results in

$$\frac{v_a}{v_w} = (\sin\theta\cos\phi - f)\sqrt{1 + \left(\frac{L}{D}\right)^2}. \tag{2.15}$$

By definition, the magnitude of the apparent wind velocity cannot be negative which constrains the reeling factor as follows

$$f < \sin\theta\cos\phi. \tag{2.16}$$

This correspond to the fundamental flight requirement that the component of the wind velocity along the tether needs to be higher than the tether reeling velocity.

2.4 Tangential kite velocity

The tangential component of the apparent wind velocity follows from Eq. (2.11) as

$$v_{a,\tau} = v_w \sqrt{(\cos\theta\cos\phi - \lambda\cos\chi)^2 + (\sin\phi + \lambda\sin\chi)^2}. \tag{2.17}$$

Another equation is obtained by combining Eqns. (2.13) and (2.14)

$$v_{a,\tau} = (\sin\theta\cos\phi - f) v_w \frac{L}{D}. \tag{2.18}$$

For the special case of $\phi = \beta = 0$, at the point of maximum traction power, this equation reduces to the relation

$$\lambda = (1-f)\frac{L}{D}, \tag{2.19}$$

which was already established in [7]. Combining Eqns. (2.17) and (2.18) and subsequently solving for tangential velocity factor λ results in

$$\lambda = a + \sqrt{a^2 + b^2 - 1 + \left(\frac{L}{D}\right)^2 (b-f)^2}, \tag{2.20}$$

with the trigonometric coefficients

$$a = \cos\theta\cos\phi\cos\chi - \sin\phi\sin\chi, \tag{2.21}$$

$$b = \sin\theta\cos\phi. \tag{2.22}$$

The tangential velocity factor illustrates the coupling of the flight velocity of the wing to the wind velocity, as discussed in Sect. 2.1. An equation for the tangential kite velocity was also derived in [3, Eq. (3)]. By definition, the tangential velocity factor λ cannot be negative. Analyzing Eq. (2.20) for this condition results in the following constraint

$$\sin\theta\cos\phi < \frac{\sqrt{1 + \left(\frac{L}{D}\right)^2 (1-f^2)} + f\left(\frac{L}{D}\right)^2}{1 + \left(\frac{L}{D}\right)^2}, \tag{2.23}$$

which indicates that there is a maximum azimuth angle ϕ_{max} and elevation angle β_{max} for physically possible flight conditions. For horizontal flight ($\chi = 90°$) in a downwind position ($\phi = 0$) Eq. (2.20) simplifies to

$$\lambda = \sqrt{\left(\frac{L}{D}\right)^2 (\sin\theta - f)^2 - \cos^2\theta}, \tag{2.24}$$

while Eq. (2.23) can be used to derive the maximum elevation angle as

$$\beta_{max} = \arccos\left(\frac{\sqrt{1+\left(\frac{L}{D}\right)^2(1-f^2)} + f\left(\frac{L}{D}\right)^2}{1+\left(\frac{L}{D}\right)^2}\right). \tag{2.25}$$

Fig. 2.5 shows the isolines of the elevation angle β as functions of course angle χ and tangential velocity factor λ for the special case of flight in a downwind position ($\phi = 0$) and representative values for lift-to-drag ratio and reeling factor. For $\beta = 0$

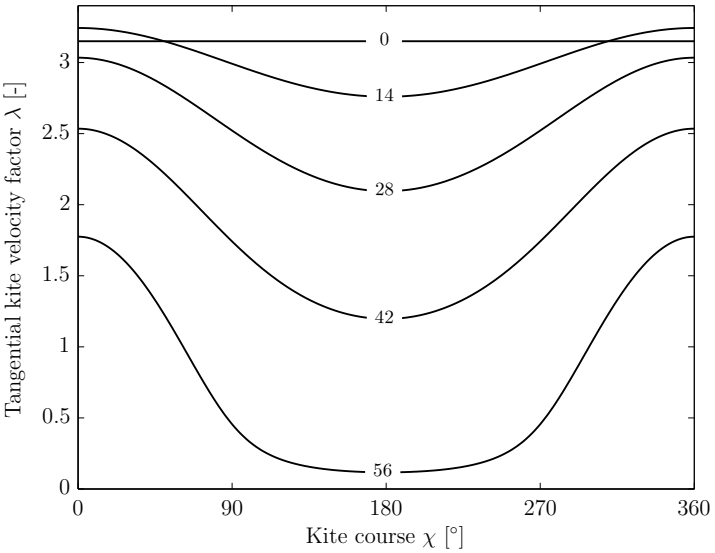

Fig. 2.5 Elevation angle $\beta[^\circ]$ as a function of kite course χ and tangential velocity factor λ for $\phi = 0$, $L/D = 5$ and $f = 0.37$.

the tangential velocity factor is constant, independent of the course angle, because the tether is aligned with the wind velocity and the tangential kite velocity is always perpendicular to the wind velocity. This is not the case anymore for non-zero elevation angles, which show a maximum value of λ at $\chi = 0$, i.e. when the kite flies downwards. This can be explained on the basis of the projection of Eq. (2.4) into the tangential plane

$$\mathbf{v}_{w,\tau} = \mathbf{v}_{a,\tau} + \mathbf{v}_{k,\tau}. \tag{2.26}$$

The tangential component of the kite velocity $\mathbf{v}_{k,\tau}$ varies by definition with the course angle χ. However, the tangential component of the wind velocity $\mathbf{v}_{w,\tau}$ depends only on the angular position (ϕ,β) of the wing and is independent of χ. According to Eq. (2.18) the magnitude of the tangential component of the apparent wind velocity $v_{a,\tau}$ is also independent of χ. This leaves only the direction of vector $\mathbf{v}_{a,\tau}$ to adjust to the varying vector $\mathbf{v}_{k,\tau}$ to fulfill Eq. (2.26). This situation is illustrated in Fig. 2.6 for different combinations of $\mathbf{v}_{a,\tau}$ and $\mathbf{v}_{k,\tau}$. The diagram clearly

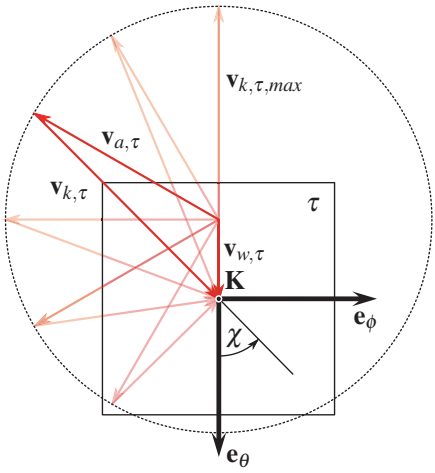

Fig. 2.6 Tangential velocity diagram for the special case of $\phi = 0$ but arbitrary value of β.

shows that for $\phi = 0$ the maximum value $v_{k,\tau,max}$ occurs at $\chi = 0$. Fig. 2.5 further shows that the average tangential kite velocity decreases with increasing elevation angle. This can be explained by the increasing misalignment of tether and wind velocity which decreases the apparent wind velocity.

2.5 Traction force

As discussed in Sect. 2.2, the assumption of quasi-steady motion of a massless kite is governed by the equilibrium of tether force $\mathbf{F}_t$ and resultant aerodynamic force $\mathbf{F}_a$

$$\mathbf{F}_t = -\mathbf{F}_a. \tag{2.27}$$

Inserting Eqns. (2.2) and (2.3) into Eq. (2.27) results in

$$F_t = \frac{1}{2}\rho C_R v_a^2 S, \tag{2.28}$$

making use of the resultant aerodynamic force coefficient

$$C_R = \sqrt{C_D^2 + C_L^2}. \tag{2.29}$$

Substituting the apparent wind velocity in Eq. (2.28) by Eq. (2.15) leads to the following equation for the normalized tether force

$$\frac{F_t}{qS} = C_R \left[1 + \left(\frac{L}{D}\right)^2\right] (\sin\theta\cos\phi - f)^2, \tag{2.30}$$

where q denotes the dynamic wind pressure

$$q = \frac{1}{2}\rho v_w^2. \tag{2.31}$$

Using Eq. (2.29) the aerodynamic coefficient term can be formulated as

$$C_R \left[1 + \left(\frac{L}{D}\right)^2\right] = C_R \left(\frac{C_R}{C_D}\right)^2. \tag{2.32}$$

Equation (2.30) has been published previously by Argatov et al. [2, Eq. (48)].

2.6 Traction power

The generated traction power is determined as the product of tether force and reeling velocity

$$P = F_t v_t. \tag{2.33}$$

Inserting the reeling factor as defined in Eq. (2.9) leads to

$$P = F_t f v_w \tag{2.34}$$

and further inserting the normalized tether force as defined Eq. (2.30) gives

$$\frac{P}{P_w S} = C_R \left[1 + \left(\frac{L}{D}\right)^2\right] f(\sin\theta\cos\phi - f)^2, \tag{2.35}$$

where P_w denotes the wind power density

$$P_w = \frac{1}{2}\rho v_w^3. \tag{2.36}$$

Equation (2.35) defines the power harvesting factor $\zeta = P/(P_w S)$ as the normalized traction power per wing surface area, also introduced as Eq. (1.10) in Chap. 1.

To determine the optimal reeling factor Eq. (2.35) is differentiated with respect to f. The root of this function defines the value f_{opt} at which the instantaneous power is maximum

$$f_{opt} = \frac{1}{3}\sin\theta\cos\phi. \tag{2.37}$$

Equation (2.37) corresponds to [2, Eq. (49)] and for the special case of $\phi = \beta = 0$ to [7, Eq. (17)]. The maximum instantaneous power follows from substituting Eq. (2.37) into Eq. (2.35)

$$\frac{P_{opt}}{P_w S} = C_R\left[1+\left(\frac{L}{D}\right)^2\right]\left(\frac{4}{27}\sin^3\theta\cos^3\phi\right). \tag{2.38}$$

For $\phi = \beta = 0$ Eq. (2.38) reduces to

$$\frac{P_{opt}}{P_w S} = \frac{4}{27}C_R\left(\frac{C_R}{C_D}\right)^2, \tag{2.39}$$

which is also given by Eq. (1.11) in Chap. 1. For larger lift-to-drag ratios C_R can be approximated by C_L such that Eq. (2.39) further simplifies to the classic result [7, Eq. (16)].

Figure 2.7 shows the isolines of instantaneous traction power P and tangential velocity factor λ as functions of reeling factor f and elevation angle β for the special case of horizontal flight in a downwind position. The power increases with decreas-

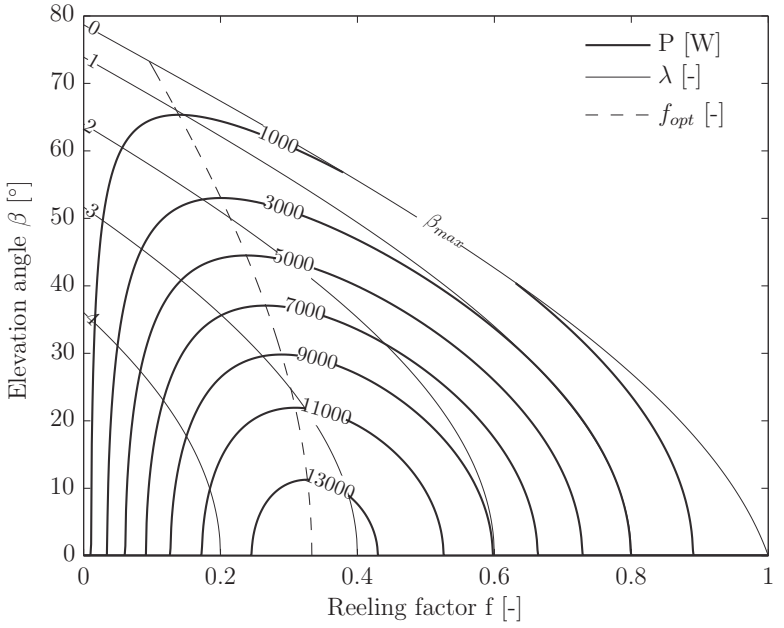

Fig. 2.7 Instantaneous traction power P and tangential velocity factor λ for $\phi = 0°$, $\chi = 90°$, $L/D = 5$, $C_L = 1$, $S = 16.7m^2$, $v_w = 7m/s$ and $\rho = 1.225kg/m^3$

ing elevation angle because the tether increasingly aligns with the wind velocity vector which effectively increases the apparent wind velocity. The depicted isolines of $P = 1000$W and 13000W correspond to power harvesting factors of $\zeta = 0.2850$ and 3.705, respectively. The maximum value $\zeta_{max} = 3.928$ occurs at $\beta = 0$ and $f = 1/3$ and is quantified by Eq. (2.39). The optimal reeling factor f_{opt} given by Eq. (2.37) is indicated by the dashed line. The tangential velocity factor λ decreases with increasing elevation angle. The minimum value isoline $\lambda = 0$ coincides with the theoretically possible maximum elevation angle β_{max}. As consequence, the top right area of the diagram represents operational conditions that can not be realized for the specific choice of wind conditions and system parameters.

2.7 Non-maneuvering wing

For continuous electricity generation, a single traction kite has to be operated in pumping cycles, alternating between traction and retraction phases. The fundamental working principles have been discussed in Chap. 1 and an implemented system is presented in Chap. 23. When terminating the crosswind flight maneuvers at the end of the traction phase the wing can be moved to an equilibrium angular position (ϕ, β) such that during reeling in, the only motion is due to the longitudinal tether velocity. For vanishing tether velocity the kite accordingly assumes a stationary position which is practical for lifting payload. In [7] the non-maneuvering flight mode is denoted as *simple kite*. For $v_{k,\tau} = 0$ Eq. (2.11) reduces to

$$\mathbf{v}_a = \begin{bmatrix} \sin\theta\cos\phi - f \\ \cos\theta\cos\phi \\ -\sin\phi \end{bmatrix} v_w, \tag{2.40}$$

with a normalized magnitude of

$$\frac{v_a}{v_w} = \sqrt{1 - 2f\sin\theta\cos\phi + f^2}. \tag{2.41}$$

Combining Eqns. (2.15) and (2.41) results in the following relation

$$\sin\theta\cos\phi = \frac{\sqrt{1 + \left(\frac{L}{D}\right)^2 (1 - f^2)} + f\left(\frac{L}{D}\right)^2}{1 + \left(\frac{L}{D}\right)^2}, \tag{2.42}$$

which is the limiting case of the constraint defined by Eq. (2.23). The parametric curves defined by Eq. (2.42) are illustrated in Fig. 2.8 for different values of L/D and a specific choice of f. Each isoline is characterized by a maximum achievable elevation and azimuth angle β_{max} and ϕ_{max}, respectively. Combining Eqns. (2.15) and (2.42) to eliminate the trigonometric coefficients leads to

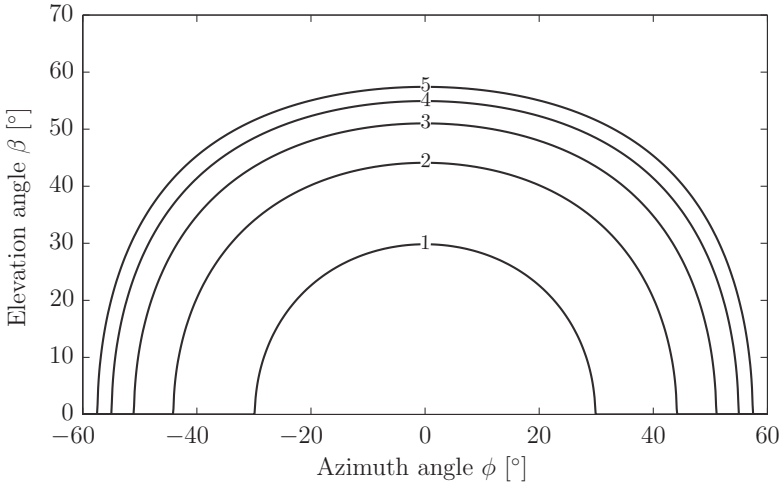

Fig. 2.8 Equilibrium flight positions for different values of L/D at a constant value of $f = 0.37$

$$\frac{v_a}{v_w} = \frac{\sqrt{1+\left(\frac{L}{D}\right)^2(1-f^2)}-f}{\sqrt{1+\left(\frac{L}{D}\right)^2}}, \tag{2.43}$$

combining Eqns. (2.28) and (2.43) to

$$\frac{F_t}{qS} = C_R \frac{\left[\sqrt{1+\left(\frac{L}{D}\right)^2(1-f^2)}-f\right]^2}{1+\left(\frac{L}{D}\right)^2}. \tag{2.44}$$

and combining Eqns. (2.34) and (2.44) to

$$\frac{P}{P_w S} = C_R \frac{f\left[\sqrt{1+\left(\frac{L}{D}\right)^2(1-f^2)}-f\right]^2}{1+\left(\frac{L}{D}\right)^2}. \tag{2.45}$$

This result has also been presented in [7]. It has to be noted, that the equilibrium positions described by Eq. (2.42) are not necessarily stable flight dynamic states of the wing [4, 9]. Static and dynamic flight dynamic stability is not in the scope of this analysis.

2.8 Traction of a ground vehicle

A kite system can also be used for ground vehicle propulsion. A fixed tether length is assumed such that the radial kite velocity $\mathbf{v}_{k,r}$ is zero. The apparent wind velocity can then be defined as follows

$$\mathbf{v}_a = \mathbf{v}_w - \mathbf{v}_p - \mathbf{v}_k, \tag{2.46}$$

where $\mathbf{v}_p$ is the additional ground vehicle velocity. It is further assumed that this velocity is constant in magnitude and direction such that additional inertial terms do not exist. Using a spherical coordinate system moving with the vehicle, the apparent wind velocity can be expressed as follows

$$\mathbf{v}_a = \begin{bmatrix} \sin\theta\cos\phi \\ \cos\theta\cos\phi \\ -\sin\phi \end{bmatrix} v_w - \begin{bmatrix} \sin\theta\cos(\psi-\phi) \\ \cos\theta\cos(\psi-\phi) \\ -\sin(\psi-\phi) \end{bmatrix} v_p - \begin{bmatrix} 0 \\ \cos\chi \\ \sin\chi \end{bmatrix} v_{k,\tau}, \tag{2.47}$$

where the course angle ψ of the ground vehicle is measured in the ground plane between ground vehicle velocity $\mathbf{v}_p$ and wind velocity $\mathbf{v}_w$. Using the definition of tangential kite velocity factor λ as given by Eq. (2.10) and the ground vehicle velocity factor

$$\xi = \frac{v_p}{v_w}, \tag{2.48}$$

the apparent wind velocity can be expressed as

$$\mathbf{v}_a = \begin{bmatrix} \sin\theta\cos\phi - \xi\sin\theta\cos(\psi-\phi) \\ \cos\theta\cos\phi - \xi\cos\theta\cos(\psi-\phi) - \lambda\cos\chi \\ -\sin\phi + \xi\sin(\psi-\phi) - \lambda\sin\chi \end{bmatrix} v_w. \tag{2.49}$$

Combining Eqns. (2.12), (2.13) and the radial component of Eq. (2.49) results in

$$v_a = [\sin\theta\cos\phi - \xi\sin\theta\cos(\psi-\phi)]\, v_w \sqrt{1+\left(\frac{L}{D}\right)^2}, \tag{2.50}$$

which is similar to [5, Eq. (3)] when neglecting the ground vehicle velocity. Combining Eqns. (2.28) and (2.50) the normalized tether force is calculated as

$$\frac{F_t}{qS} = C_R\left[1+\left(\frac{L}{D}\right)^2\right][\sin\theta\cos\phi - \xi\sin\theta\cos(\psi-\phi)]^2. \tag{2.51}$$

The force component in direction of the ground vehicle velocity describes the propulsive force

$$F_p = F_t\sin\theta\cos(\psi-\phi). \tag{2.52}$$

Combining Eqns. (2.51) and (2.52) results in

$$\frac{F_p}{qS} = C_R \left[1 + \left(\frac{L}{D}\right)^2\right] [\sin\theta\cos\phi - \xi \sin\theta \cos(\psi - \phi)]^2 \sin\theta \cos(\psi - \phi), \quad (2.53)$$

with the restriction

$$\xi < \frac{\cos\phi}{\cos(\psi - \phi)}, \quad (2.54)$$

which means that the projection of the ground vehicle velocity onto the tether cannot be larger than that of the wind velocity, because this would result in a negative apparent wind velocity. For pure downwind traction ($\phi = 0$) this simplifies to

$$\frac{F_p}{qS} = C_R \left[1 + \left(\frac{L}{D}\right)^2\right] (1 + \xi \cos\psi)^2 \sin^3\theta \cos\psi. \quad (2.55)$$

Figure 2.9 shows isolines of the ground vehicle velocity factor ξ as functions of azimuth angle and propulsion force for a specific ground vehicle course. The diagram

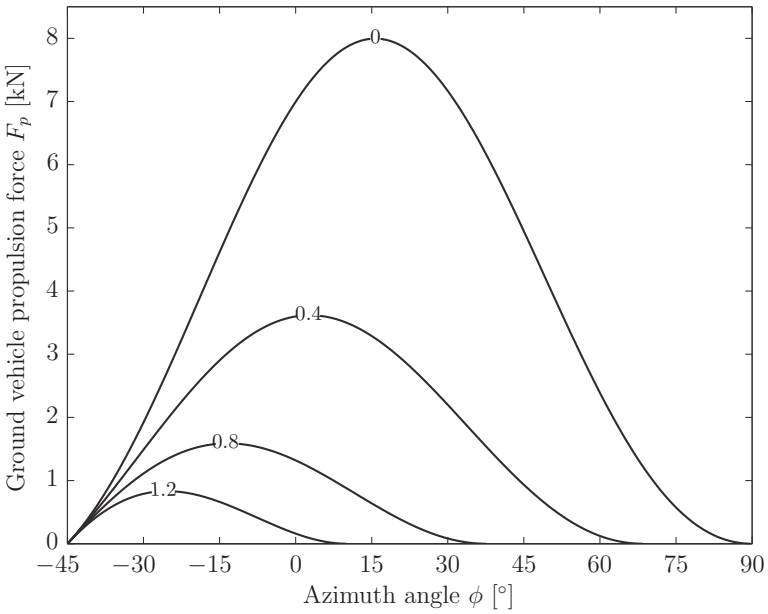

Fig. 2.9 Ground vehicle velocity factor ξ as a function of azimuth angle ϕ and ground vehicle propulsion force F_p. The specific conditions are given by $\psi = 45°$, indicated by the dashed line, $\beta = 25°$, $L/D = 5$, $C_L = 1$, $S = 16.7\text{m}^2$, $v_w = 7\text{m/s}$ and $\rho = 1.225\text{kg/m}^3$.

clearly indicates the optimal azimuth angle ϕ_{opt} for achieving a maximum ground vehicle propulsion force F_p. For increasing ground vehicle velocity, the optimum shifts to the side of the wind window. This can be explained by the fact that the

ground vehicle velocity reduces the wind velocity component parallel to the ground vehicle velocity.

A similar effect is illustrated in Fig. 2.10 which shows isolines of the ground vehicle velocity factor ξ as functions of ground vehicle course angle and propulsion force at the optimal azimuth angle. The diagram indicates that an increasing ground vehicle velocity shifts the optimum ground vehicle course angle ψ to higher course angles. This effect is also described in [11].

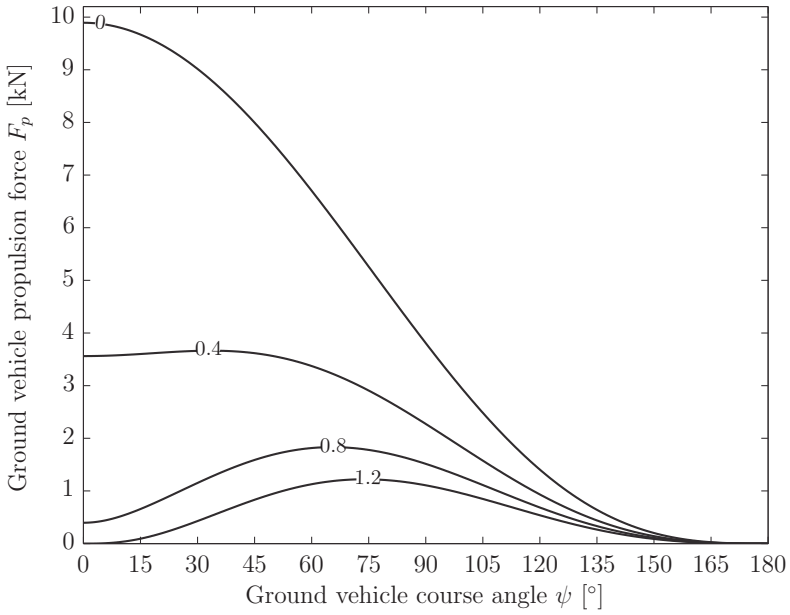

Fig. 2.10 Ground vehicle velocity factor ξ as a function of ground vehicle course angle ψ and ground vehicle propulsion force F_p for $\phi = \phi_{opt}$. The specific conditions are $\beta = 25°$, $L/D = 5$, $C_L = 1$, $S = 16.7\text{m}^2$, $v_w = 7\text{m/s}$ and $\rho = 1.225\text{kg/m}^3$.

2.9 Gravitational and inertial force corrections

The idealized theory presented in the previous sections does not account for the mass of the kite. In reality, the non-vanishing mass of the airborne components introduces gravitational and inertial forces. These effects have been analyzed in [1, Eq. (7.8)] considering an arbitrary predefined trajectory with constant tether length. Using spherical coordinates the gravitational force can be expressed as

$$\mathbf{F}_g = m \begin{bmatrix} -\cos\theta \\ \sin\theta \\ 0 \end{bmatrix} g, \tag{2.56}$$

with mass m and gravitational constant g. The inertial force is given by

$$\mathbf{F}_i = -m \begin{bmatrix} \ddot{r} - r\dot{\theta}^2 - r\dot{\phi}^2 \sin^2\theta \\ r\ddot{\theta} + 2\dot{r}\dot{\theta} - r\dot{\phi}^2 \sin\theta\cos\theta \\ r\ddot{\phi}\sin\theta + 2\dot{r}\dot{\phi}\sin\theta + 2r\dot{\theta}\dot{\phi}\cos\theta \end{bmatrix}, \tag{2.57}$$

where the first derivatives can be expressed as follows

$$\dot{r} = f v_w, \tag{2.58}$$

$$\dot{\theta} = \frac{\lambda v_w}{l_t}\cos\chi, \tag{2.59}$$

$$\dot{\phi} = \frac{\lambda v_w}{l_t}\frac{\sin\chi}{\sin\theta}, \tag{2.60}$$

using the tether length as a substitute for the radial coordinate

$$r = l_t. \tag{2.61}$$

Following the assumption of a quasi-steady motion, the time derivatives of the radial and tangential kite velocity $v_{k,r}$ and $v_{k,\tau}$, respectively, are small. As consequence, the second derivatives can be evaluated as

$$\ddot{r} = 0, \tag{2.62}$$

$$\ddot{\theta} = -\dot{\theta}\left(\frac{\dot{r}}{l_t} + \dot{\chi}\tan\chi\right), \tag{2.63}$$

$$\ddot{\phi} = -\dot{\phi}\left(\frac{\dot{r}}{l_t} - \dot{\chi}\frac{1}{\tan\chi} + \dot{\theta}\frac{1}{\tan\theta}\right). \tag{2.64}$$

Extending the force balance formulated in Eq. (2.27) by the effects of gravity and inertia gives

$$\mathbf{F}_t = -\mathbf{F}_a - \mathbf{F}_g - \mathbf{F}_i. \tag{2.65}$$

The gravitational and inertial forces both have tangential components which distort the alignment of aerodynamic force and tether force. For this reason the force and velocity diagrams are not geometrically similar anymore. This is illustrated in Fig. 2.11 considering only the effect of gravity in $-\mathbf{e}_z$ direction. Therefore, the fundamental relation given by Eq. (2.13) is not valid anymore, which means that kinematic ratio $v_{a,\tau}/v_{a,r}$ can not be substituted anymore by the lift-to-drag ratio L/D. The apparent wind velocity $\mathbf{v}_a$ is given by Eq. (2.11), however, the tangential kite velocity factor λ now takes the form

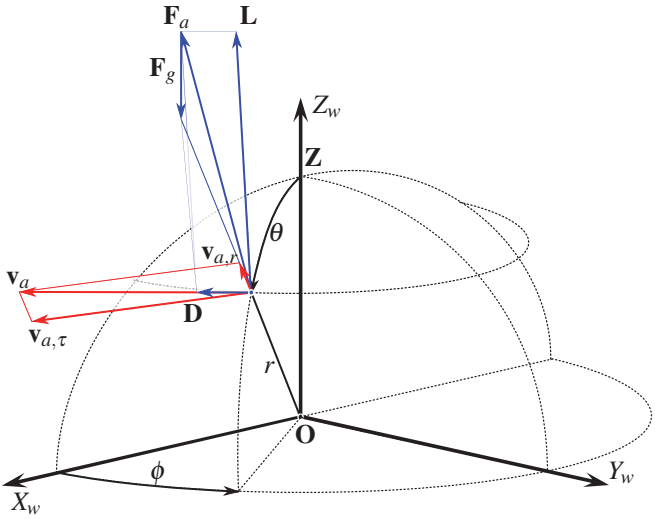

Fig. 2.11 Steady force equilibrium considering the effect of gravity.

$$\lambda = a + \sqrt{a^2 + b^2 - 1 + \left(\frac{v_{a,\tau}}{v_{a,r}}\right)^2 (b-f)^2}, \tag{2.66}$$

with the trigonometric coefficients a and b defined in Eqns. (2.21) and (2.22). Accordingly, the magnitude of the apparent wind velocity is formulated as

$$v_a = (\sin\theta\cos\phi - f) v_w \sqrt{1 + \left(\frac{v_{a,\tau}}{v_{a,r}}\right)^2}. \tag{2.67}$$

Defining the aerodynamic force as

$$F_a = \frac{1}{2}\rho C_R v_a^2 S \tag{2.68}$$

and expressing the apparent wind velocity by Eq. (2.67) results in

$$\frac{F_a}{qS} = C_R \left[1 + \left(\frac{v_{a,\tau}}{v_{a,r}}\right)^2\right] (\sin\theta\cos\phi - f)^2. \tag{2.69}$$

Physically feasible flight conditions require a kinematic ratio $v_{a,\tau}/v_{a,r}$ for which the aerodynamic force balances the tangential components of the gravitational and inertial forces.

The final part of this section describes an iterative solution procedure for the kinematic ratio. Because the tether force acts in radial direction, the tangential components of the aerodynamic force need to balance the tangential components of the gravitational and inertial forces, which is expressed by

$$F_{a,\theta} = -F_{g,\theta} - F_{i,\theta}, \tag{2.70}$$

$$F_{a,\phi} = -F_{i,\phi}. \tag{2.71}$$

The radial component is determined by

$$F_{a,r} = \sqrt{F_a^2 - F_{a,\theta}^2 - F_{a,\phi}^2}, \tag{2.72}$$

and Eqns. (2.69), (2.70) and (2.71) are used to substitute the force terms on the right hand side. Finally, the definition of the aerodynamic drag force

$$\mathbf{D} = \frac{\mathbf{F}_a \cdot \mathbf{v}_a}{v_a^2} \mathbf{v}_a \tag{2.73}$$

is inserted into Eq. (2.1) to obtain the following expression for the lift-to-drag ratio

$$\frac{L}{D} = \sqrt{\left(\frac{F_a v_a}{\mathbf{F}_a \cdot \mathbf{v}_a} \right)^2 - 1}, \tag{2.74}$$

which can be used to determine the kinematic ratio iteratively. Figure 2.12 shows

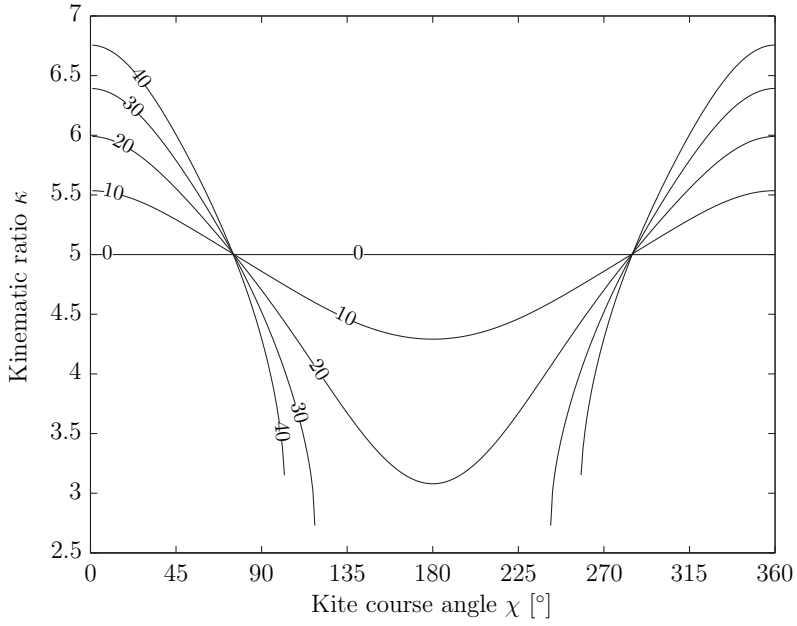

Fig. 2.12 Kite mass m as function of course angle χ and kinematic ratio $v_{a,\tau}/v_{a,r}$ for $\beta = 25°$, $f = 0.37$, $L/D = 5$, $C_L = 1$, $S = 16.7\text{m}^2$, $v_w = 7\text{m/s}$ and $\rho = 1.225\text{kg/m}^3$.

computed isolines of the kite mass as functions of the kite course angle and the kinematic ratio. The effect on the instantaneous traction power can be significant because the aerodynamic force depends quadratically on the kinematic ratio, as indicated by Eq. (2.69). The limiting case of a massless kite recovers Eq. (2.13) and the kinematic ratio equals the constant value of the lift-to-drag ratio. For horizontal flight ($\chi = 90°$ and $\chi = 270°$) the kinematic ratio is always lower than the lift-to-drag ratio. With increasing mass of the kite the kinematic ratio increases for downwards flight and decreases for upwards flight. However, the increase for downwards flight is weaker than the decrease for upwards flight. When exceeding a certain mass limit the algorithm fails to identify a physical solution for the upward flight region.

The effect of gravity and inertia on continuous power generation can be significant for the following reasons. Firstly, Fig. 2.12 indicates that the mean kinematic ratio along a closed-loop trajectory is lower than the lift-to-drag ratio. Secondly, when the kinematic ratio is lower, the quasi-steady flight velocity of the wing is lower. This means that the upward flying regions of a closed-loop trajectory require more time than the downward flying regions. These conclusions are contradicting the statement in [2] that the kinematic ratio alternates on a closed-loop trajectory and that the effect on the mean power can therefore be neglected.

Figure 2.13 illustrates the effect of kite mass of 20kg on the traction power for the special case of horizontal flight in a downwind position ($\phi = 0$). Compared to

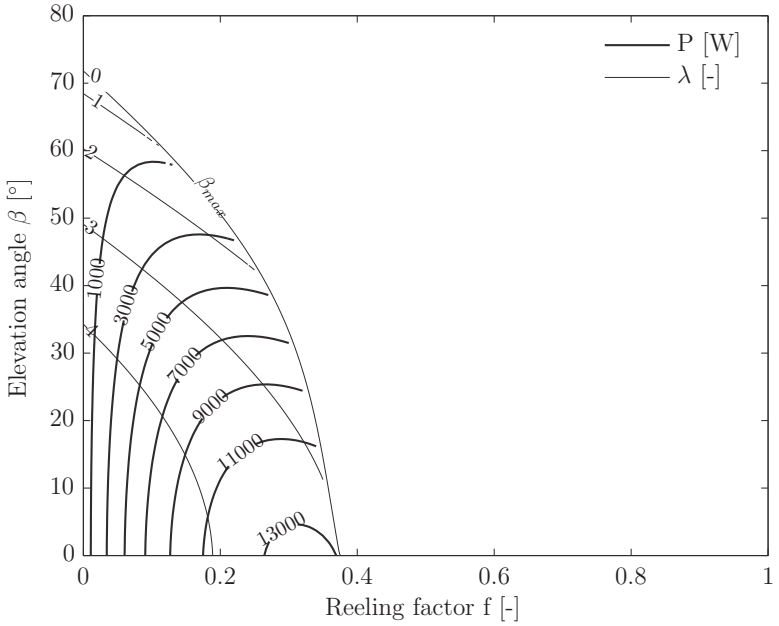

Fig. 2.13 Instantaneous traction power P and tangential velocity factor λ for $m = 20$kg, $\phi = 0°$, $\chi = 90°$, $L/D = 5$, $C_L = 1$, $S = 16.7\text{m}^2$, $v_w = 7$m/s and $\rho = 1.225\text{kg/m}^3$

Fig. 2.7 it can be noted that an operation for reeling factors $f > 0.37$ is not feasible anymore. Also, the isolines of traction power are shifted to lower values of the elevation angle. Within the frame of this steady analysis it can be concluded that an increasing mass of the airborne components always decreases the available traction power of the wing.

2.10 Conclusion

The flight velocity $\mathbf{v}_k$ of a tethered wing for specific wind conditions and operational parameters can be described analytically by means of a steady analysis. Neglecting the effects of gravity and inertia, Eq. (2.15) states the apparent wind velocity v_a, Eq. (2.30) the tether force F_t and Eq. (2.35) the instantaneous traction power P of a wing which flies on an arbitrary predefined trajectory.

The maximum instantaneous traction power is associated with an optimal reeling factor f_{opt} which is given by Eq. (2.37) as one-third of the wind velocity component in the direction of the tether. The corresponding value P_{opt} is given by Eq. (2.38). As consequence, generating a maximum traction power requires lower reeling velocities when the wing deviates from the maximum power point, i.e. the center of the wind window. The instantaneous traction power depends linearly on the projected surface area of the wing, quadratically on the lift-to-drag ratio and cubically on the wind velocity. For the purpose of this analysis, it is assumed that the resulting aerodynamic coefficient C_R is independent of the lift-to-drag ratio.

When including the effects of gravity and inertia in the analysis, an iterative solution procedure has to be employed. An increasing mass of the airborne components always decreases the available traction power of the wing.

For a small kite power system in the kW-range the instantaneous power in the traction phase is around 10kW for $S = 16.7\text{m}^2$, $L/D = 5$, $v_w = 7\text{m/s}$ and $\beta = 25°$. However future systems can be in the MW-range, e.g. a maximum instantaneous traction power of 1.2MW is obtained for $S = 100\text{m}^2$, $L/D = 10$, $v_w = 12\text{m/s}$ and $\beta = 25°$.

References

1. Argatov, I., Silvennoinen, R.: Asymptotic modeling of unconstrained control of a tethered power kite moving along a given closed-loop spherical trajectory. Journal of Engineering Mathematics **72**(1), 187–203 (2012). doi: 10.1007/s10665-011-9475-3
2. Argatov, I., Rautakorpi, P., Silvennoinen, R.: Estimation of the mechanical energy output of the kite wind generator. Renewable Energy **34**(6), 1525–1532 (2009). doi: 10.1016/j.renene.2008.11.001
3. Argatov, I., Silvennoinen, R.: Energy conversion efficiency of the pumping kite wind generator. Renewable Energy **35**(5), 1052–1060 (2010). doi: 10.1016/j.renene.2009.09.006
4. Breukels, J.: An Engineering Methodology for Kite Design. Ph.D. Thesis, Delft University of Technology, 2011. http://resolver.tudelft.nl/uuid:cdece38a-1f13-47cc-b277-ed64fdda7cdf

5. Dadd, G. M., Hudson, D. A., Shenoi, R. A.: Determination of kite forces using three-dimensional flight trajectories for ship propulsion. Renewable Energy **36**(10), 2667–2678 (2011). doi: 10.1016/j.renene.2011.01.027
6. Houska, B., Diehl, M.: Optimal control for power generating kites. In: Proceedings of the 9th European Control Conference, pp. 3560–3567, Kos, Greece, 2–5 July 2007. http://www.kuleuven.be/optec/files/Houska2007.pdf
7. Loyd, M. L.: Crosswind kite power. Journal of Energy **4**(3), 106–111 (1980). doi: 10.2514/3.48021
8. Schmehl, R.: Large-scale power generation with kites. Journal of the Society of Aerospace Engineering Students VSV Leonardo da Vinci March, 21–22 (2012). http://resolver.tudelft.nl/uuid:84b37454-5790-4708-95ef-5bc2c60be790
9. Terink, E. J., Breukels, J., Schmehl, R., Ockels, W. J.: Flight Dynamics and Stability of a Tethered Inflatable Kiteplane. AIAA Journal of Aircraft **48**(2), 503–513 (2011). doi: 10.2514/1.C031108
10. Wellicome, J. F.: Some comments on the relative merits of various wind propulsion devices. Journal of Wind Engineering and Industrial Aerodynamics **20**(1–3), 111–142 (1985). doi: 10.1016/0167-6105(85)90015-7
11. Williams, P., Lansdorp, B., Ockels, W.: Optimal Crosswind Towing and Power Generation with Tethered Kites. AIAA Journal of Guidance, Control, and Dynamics **31**(1), 81–93 (2008). doi: 10.2514/1.30089

http://www.springer.com/978-3-642-39964-0

Airborne Wind Energy
Ahrens, U.; Diehl, M.; Schmehl, R. (Eds.)
2013, XXIII, 611 p. 337 illus., 161 illus. in color.,
Hardcover
ISBN: 978-3-642-39964-0